DYNA
http://dyna.medellin.unal.edu.co/

UNIVERSIDAD NACIONAL DE COLOMBIA

A reliability model for non-isothermal isotropic damages

Allan Jonathan da Silva & Felipe do Carmo Amorim

Centro Federal de Educação Tecnológica Celso Suckow da Fonseca (CEFET/RJ), Itaguaí, Rio de Janeiro, Brasil. allan.jonathan@cefet-rj.br, felipe.amorim@cefet-rj.br

Received: September 27th, 2023. Received in revised form: April 2nd, 2024. Accepted: April 8th, 2024.

Abstract
This study introduces a novel lifetime distribution originating from the Neyman Type A distribution. We built a Neyman Type A counting process and developed a survival function. Some statistical properties of the new distribution were presented, such as the resulting humped hazard function and its convergence. An accelerated test model structure with Arrhenius law was specified, and the effects of different accelerating stresses were analyzed. The hazard function implied by the model is inversely proportional to the stress, which results in interesting features and provides an efficient approach to describe the lifespan phenomena of some engineering metals and bulbs under low temperatures. The estimation of parameters of the accelerated model by maximum likelihood, mean time to failure, and expected number of failures are discussed in the numerical experiments.

Keywords: reliability; Neyman type A distribution; accelerated life tests.

Un modelo de confiabilidad para daños isotrópicos no isotérmicos

Resumen
Este artículo presenta una nueva distribución de vida útil que se origina a partir de la distribución de Neyman Tipo A. Construimos el proceso de conteo de Neyman Tipo A y desarrollamos la función de supervivencia. Se presentan algunas propiedades estadísticas de la nueva distribución, como la función de riesgo resultante en forma de joroba y su convergencia. Se especifica una estructura de modelo de prueba acelerada con la ley de Arrhenius, y se analizan los efectos de diferentes tensiones acelerantes. La función de riesgo implicada por el modelo es inversamente proporcional al estrés, lo que resulta en características interesantes: el modelo proporciona un enfoque eficiente para describir los fenómenos de vida útil de algunos metales de ingeniería y bombillas a bajas temperaturas. Se discute la estimación de parámetros del modelo acelerado mediante máxima verosimilitud, el tiempo medio hasta la falla y el número esperado de fallas en experimentos numéricos.

Palabras clave: confiabilidad; distribución de Neyman tipo A; pruebas de vida aceleradas.

1 Introduction

Understanding how components and systems age is of academic and industrial interest. The development of the lifetime distribution is the core of reliability engineering and related areas. From statistical distributions, many important concepts such as the hazard function, mean time to failure, probability of failure, and mean residual life can be obtained. There is a vast amount of modern literature supporting the component's lifetime. The reliability engineering basics can be found in [1,2]. The accelerated life test models can be found in [3]. Many recent books discuss warranty policies, such as [4-9] discussed maintenance policies, costs associated with imperfect repairs, and maintenance optimization with variable recovery factors, respectively.

Many models discuss the lifetime data distributions. Classical exponential, Weibull, and lognormal distributions have been extensively studied. These models can derive various hazard functions. [3] also found many life-stress relationships, such as Arrhenius and inverse power laws, to address the accelerated life test problem. In this context, physical laws are merged with statistical distributions to describe the failure behavior in distinct stress scenarios. In general, the higher the stress level, the lower the product performance and mean time to failure. Arrhenius's law, for example, inversely relates the lifespan to thermal stress. The inverse-power law is the same for non-thermal stresses, such

How to cite: da Silva, A.J. and Amorim, F.C., A reliability model for non-isothermal isotropic damages. DYNA, 91(232), pp. 66-76, April - June, 2024.

as voltage or vibration. The Eyring model is typically used for temperature- or humidity-accelerated stresses [3].

Nonetheless, some types of failure occur in lower-temperature environments. Cold weather tends to wear fluorescent bulbs and shorten their lifespans. Steels suffer from low temperature brittle fatigue. Aircraft and chemical processing equipment are required to operate at low temperatures, and the behavior of metals needs to be considered. Jae Myung Lee, the Guest Editor of the Special Issue "Low-Temperature Behavior of Metals" of the Metals journal, stated in [10]: "*Many engineering metals become brittle at low temperatures so that the structures fabricated using these materials may fracture or fail unexpectedly when subjected to stress levels at which the performance may be satisfactory under normal temperatures.*"

In general, the increase in the tensile and yield strengths at low temperatures is characteristic of metals. Extremely low temperatures may reduce the toughness. The transition temperature at which brittle fracture occurs is lowered by a series of characteristics, such as a decrease in the carbon content or grain size and an increase in the nickel or manganese content [11].

Notably, the behavior of metals at low temperatures is not limited to traditional crystalline metals. Brittle metallic glasses, such as Mg-based bulk metallic glasses, can also exhibit brittle behavior at low temperatures. However, even in these brittle glasses, there are indications of a "ductile" fracture mechanism, as observed through the presence of a dimple structure at the fracture surface [11].

The development of special materials that are resistant to low temperatures to store and transport hydrogen, for example, is a matter of concern. Many studies have discussed low-temperature embrittlement and fracture of metals, such as [12-17] showed that the impact toughness of locomotive wheel steel at $-60°$ test temperature has decreased three times in relation to temperatures from $-20°$ to $20°$. In the investigation of a Pb-free circuit board applied for space exploration by [18], it was shown that the ball grid array solder joint changed from ductile to brittle over the range of $-70°$ to $-80°$.

This study's novel application of a new probability distribution in reliability modeling is contextualized within the broader field of material failure analysis under extreme conditions such as low temperatures. Recent studies, such as [19], have explored superposition-based predictions of creep in polymer films at cryogenic temperatures, emphasizing the need for predictive models in environments where traditional testing is challenging. Similarly, [20] investigated the strain-hardening behavior of AISI 304 stainless steel at varying temperatures, highlighting the influence of temperature on the mechanical properties and fracture morphology. [21] discussed the computational limitations of the five main creep failure models. Furthermore, research by [22-24] has delved into the complexities of material behaviors under stress and temperature variations, revealing intricate patterns of mechanical response and failure mechanisms that are crucial for advanced engineering applications. Our model extends these discussions by providing a robust statistical framework that captures the risk failure behaviors of metallic materials at low temperatures, offering significant insights compared to existing methods. By integrating the principles observed in these studies, our approach enhances the predictive accuracy of material failure models, facilitating a more reliable design and assessment of materials for low-temperature applications.

This study aims to introduce a novel approach in reliability engineering by adapting the Neyman Type A distribution to analyze material failures under low-temperature conditions, a prevalent scenario in engineering applications. Unlike classical physico-statistical distributions such as Weibull and log-normal distributions, which primarily focus on high-stress behaviors, the Neyman Type A distribution provides a unique and robust tool for understanding and predicting failure behaviors in cold environments where materials, especially metals, exhibit brittle fractures and low-temperature fatigue. This work pioneered the use of the Neyman Type A distribution in reliability engineering, offering new insights into the failure behavior of metals in cold climates and establishing a new life-stress relationship. The chosen distribution not only captures the nuances of temperature-dependent failure rates but also features a distinctive hump-shaped hazard function that accurately defines the probability of early failures. Unlike other common distributions, it stabilizes at a non-zero constant failure rate, thus providing a strong justification for its specific application in studying metallic material failures.

The remainder of this paper is organized as follows. Section 2 defines the discrete process and introduces the counting process derived from the Neyman type-A distribution. Section 3 considers the properties of the new lifetime distribution, such as the hazard function and its maximum-likelihood estimators. A life stress model is introduced in Section 4, the properties of the new distribution are discussed, and simulations are performed. Finally, Section 5 concludes the study and discusses future work.

2 Neyman type A distribution

Consider a Poisson distribution for which the Poisson parameter $\Theta=\phi\theta$, where ϕ is a constant, and θ has a Poisson distribution with parameter λ. The outcome distribution is known as Neyman type A probability distribution [25]. This probability distribution has found applications in a diverse range of areas, ranging from biological systems [26] to the modeling of natural disasters [27]. A detailed discussion of the mixture distributions can be found in [28].

The characteristic function of the Neyman type A (NTA) probability distribution is given by

$$\hat{f}(u;\lambda,\phi) = \mathrm{e}^{\left[\lambda\left(\mathrm{e}^{\phi\left(\mathrm{e}^{iu}-1\right)}-1\right)\right]}. \tag{1}$$

The cumulant generating function of (1) is given by

$$h(u) = \left[\lambda\left(\mathrm{e}^{\phi\left(\mathrm{e}^{iu}-1\right)}-1\right)\right] \tag{2}$$

and the cumulants

$$\begin{gathered} c_1 = \lambda\phi,\ c_2 = \lambda\phi(1+\phi), \\ c_4 = \lambda\phi(1+7\phi+6\phi^2+\phi^3), \end{gathered} \tag{3}$$

calculated according to [29].

The approximation given by the COS method in [30] is particularly useful when the probability mass function is difficult to manipulate, its cumulative function has no analytical solution, and/or the function itself does not exist in an explicit form. In such cases, we may resort to the Fourier cosine series given that we know the corresponding characteristic function.

Figs. 1 and 2 depict the approximation of the Neyman type-A probability function via the Fourier Series. The local peaks at 0,25,50,76,103,129,153 and 173 for the parameters $\lambda = 7$ and $\phi = 25$ which highlight the multimodality of the distribution, were discussed by [31].

An advantage of the solution via Fourier series is that the distribution is well approximated with a finite number of cosine terms, in contrast to Neyman's type-A analytical probability mass function given by

$$\mathbb{P}\{X = x\} = \frac{\mathrm{e}^{-\lambda}\phi^x}{x!}\sum_{j=0}^{\infty}\frac{\left(\lambda \mathrm{e}^{-\phi}\right)^j j^x}{j!},\ x = 0,1,\ldots, \tag{4}$$

which has an infinite sum for each x and a factorial function. The latter is a computational challenge for large values of x. For example, the reliability of redundant equipment, desired in terms of the probability of r or fewer failures for a fixed period of time, is given by

$$R(t) = \sum_{x=0}^{r}\mathbb{P}\{X = x\} = \sum_{x=0}^{r}\left[\frac{\mathrm{e}^{-\lambda}\phi^x}{x!}\sum_{j=0}^{\infty}\frac{\left(\lambda \mathrm{e}^{-\phi}\right)^j j^x}{j!}\right], \tag{5}$$

which inherits the computational challenges of Eq. (4).

Definition 1. The counting process N(t) derived from the NTA distribution has a probability distribution given by

$$\mathbb{P}\{N(t) = x\} = \frac{\mathrm{e}^{-\lambda t}(\phi t)^x}{x!}\sum_{j=0}^{\infty}\frac{\left(\lambda t \mathrm{e}^{-(\phi t)}\right)^j j^x}{j!},\ x = 0,1\ldots \tag{6}$$

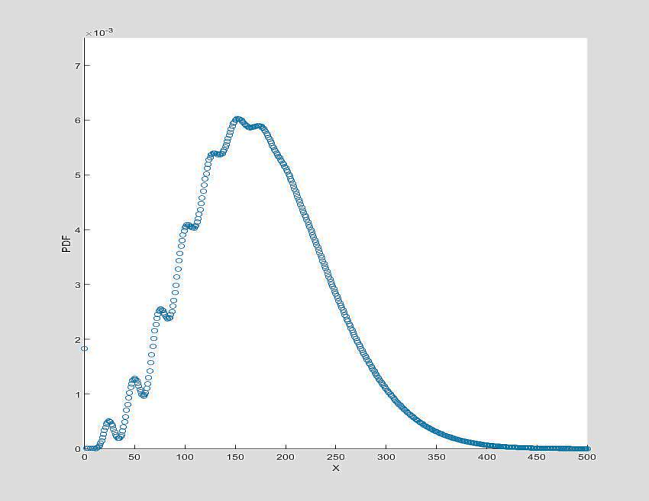

Figure 1. Neyman type A probability mass function.
Source: Authors.

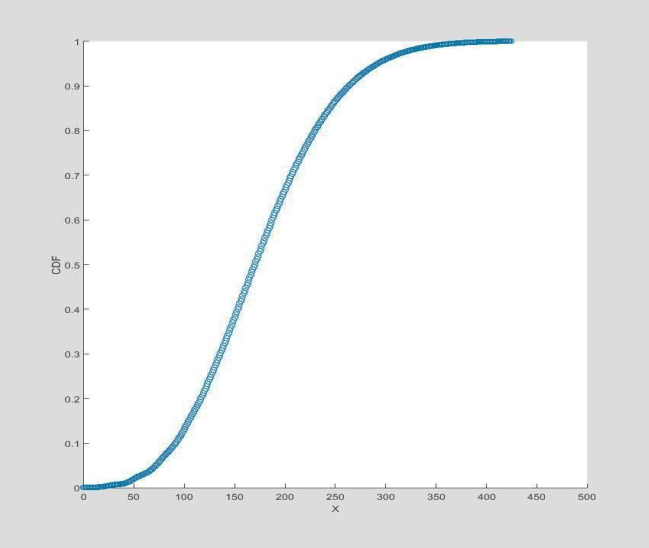

Figure 2. Neyman type A probability cumulative distribution.
Source: Authors.

In other words, for fixed parameters λ and ϕ, the probability of random variable N(t) being equal to x at time t is given by (6). Note that, as shown in [25], for the discrete random variable, $\mathbb{P}\{N(0) = 0\} = 1$.

3 Neyman type A Reliability function

This section proposes closed-form expressions of the reliability model derived from the Neyman type A counting process, their derived functions and associated properties, and the maximum likelihood estimators.

Theorem 1. The reliability (survival probability) function derived from the NTA counting process (6) is governed by:

$$R(t) = \mathrm{e}^{-\lambda t + \lambda t \mathrm{e}^{-\phi t}}. \tag{7}$$

Proof. The probability of no arrival until time t is

$$\begin{aligned}\mathbb{P}\{N(t) = 0\} &= \frac{\mathrm{e}^{-\lambda t}(\phi t)^0}{0!}\sum_{j=0}^{\infty}\frac{\left(\lambda t \mathrm{e}^{-(\phi t)}\right)^j j^0}{j!} \\ &= \mathrm{e}^{-\lambda t + \lambda t \mathrm{e}^{-\phi t}} = R(t).\end{aligned} \tag{8}$$

Eq. (8) provides the reliability function obtained from the NTA counting process. Note that $R(0) = 1$ and

$$\begin{aligned}&\lim_{t\to\infty}\mathrm{e}^{-\lambda t + \lambda t \mathrm{e}^{-\phi t}} \\ &= \lim_{t\to\infty}\mathrm{e}^{-\lambda t}\mathrm{e}^{\lambda t \mathrm{e}^{-\phi t}} \\ &= \lim_{t\to\infty}\frac{\mathrm{e}^{\lambda t \mathrm{e}^{-\phi t}}}{\mathrm{e}^{\lambda t}} \\ &= \lim_{t\to\infty}\frac{\mathrm{e}^{\frac{\lambda t}{\mathrm{e}^{\phi t}}}}{\mathrm{e}^{\lambda t}} \\ &= \frac{\lim_{t\to\infty}\mathrm{e}^{\frac{\lambda t}{\mathrm{e}^{\phi t}}}}{\lim_{t\to\infty}\mathrm{e}^{\lambda t}} = \frac{\mathrm{e}^0}{\infty} = \frac{1}{0} = 0,\end{aligned} \tag{9}$$

which agrees with the reliability axioms.

Corollary 1. If the reliability function is given by

$$R(t) = \mathrm{e}^{-\lambda t+\lambda t\mathrm{e}^{-\phi t}}, \tag{10}$$

then, its associated probability density function is given by

$$f(t) = \lambda\left(\mathrm{e}^{\phi t} + \phi t - 1\right)\mathrm{e}^{-\lambda t-\phi t+\lambda t\mathrm{e}^{-\phi t}}. \tag{11}$$

Consequently, the hazard rate is given by

$$h(t) = \lambda\left(\mathrm{e}^{\phi t} + \phi t - 1\right)\mathrm{e}^{-\phi t} \tag{12}$$

Proof. Let

$$R(t) = \mathrm{e}^{-\lambda t+\lambda t\mathrm{e}^{-\phi t}}. \tag{13}$$

The cumulative distribution function is given by $F(t) = 1 - R(t)$. Therefore, the probability density function is given by

$$\begin{aligned}\frac{dF(t)}{dt} &= \frac{d(1-R(t))}{dt}\\ &= \frac{d\left(1-\mathrm{e}^{-\lambda t+\lambda t\mathrm{e}^{-\phi t}}\right)}{dt}\\ &= \lambda\left(\mathrm{e}^{\phi t} + \phi t - 1\right)\mathrm{e}^{-\lambda t-\phi t+\lambda t\mathrm{e}^{-\phi t}} = f(t).\end{aligned} \tag{14}$$

The hazard rate is simply given by

$$\begin{aligned}h(t) &= \frac{f(t)}{R(t)}\\ &= \frac{\lambda\left(\mathrm{e}^{\phi t} + \phi t - 1\right)\mathrm{e}^{-\lambda t-\phi t+\lambda t\mathrm{e}^{-\phi t}}}{\mathrm{e}^{-\lambda t+\lambda t\mathrm{e}^{-\phi t}}}\\ &= \lambda\left(\mathrm{e}^{\phi t} + \phi t - 1\right)\mathrm{e}^{-\phi t}\end{aligned} \tag{15}$$

The hump-shaped behavior of the hazard function is similar to that implied by the lognormal distribution. It initially increases, reaches a maximum, and then decreases toward a constant value. The following two corollaries clarify this issue.

Corollary 2. The NTA hazard function (12) is a humped model.

Proof. Note that the derivative of the hazard function given by

$$\frac{\partial h(t)}{\partial t} = \lambda\mathrm{e}^{-\phi t}\left(f\mathrm{e}^{\phi t} + \phi\right) - \phi\lambda\mathrm{e}^{-\phi t}\cdot\left(\mathrm{e}^{\phi t} + \phi t - 1\right) \tag{16}$$

8 da Silva and Amorim

finds root at $t^* = \frac{2}{\phi}$. Since that $\lambda > 0$, and

$$\frac{\partial^2 h(t)}{\partial t^2} = \phi^2\lambda(\phi t - 3)\left(\mathrm{e}^{-\phi t}\right) \tag{17}$$

we have that

$$\frac{\partial^2 h(t^*)}{\partial t^2} = -\phi^2\lambda\mathrm{e}^{-2}. \tag{18}$$

So, the NTA hazard function finds its maximum at t^*.

Corollary 3. The NTA hazard function converges to λ in the long run.

Proof. If the hazard function is given by

$$h(t) = \lambda\left(\mathrm{e}^{\phi t} + \phi t - 1\right)\mathrm{e}^{-\phi t}, \tag{19}$$

then

$$\begin{aligned}&\lim_{t\to\infty}\lambda\left(\mathrm{e}^{\phi t} + \phi t - 1\right)\mathrm{e}^{-\phi t}\\ &\lambda\lim_{t\to\infty}\left(\mathrm{e}^{\phi t} + \phi t - 1\right)\mathrm{e}^{-\phi t}\\ &\lambda\lim_{t\to\infty}\left(1 + \phi t\mathrm{e}^{-\phi t} - \mathrm{e}^{-\phi t}\right)\\ &\lambda\left(\lim_{t\to\infty}1 + \lim_{t\to\infty}\phi t\mathrm{e}^{-\phi t} - \lim_{t\to\infty}\mathrm{e}^{-\phi t}\right)\\ &\lambda\left(1\lim_{t\to\infty}1 + 0\lim_{t\to\infty}\phi t\mathrm{e}^{-\phi t} - 0\lim_{t\to\infty}\mathrm{e}^{-\phi t}\right) = \lambda\end{aligned} \tag{20}$$

Fig. 3 depicts the probability density, Fig. 4 shows the reliability, and Fig. 5 shows the hazard rate functions. We may note an increasing hazard rate up to a certain point in time, namely $\frac{2}{\phi}$, where the function starts to decrease and stabilizes at a constant rate. In the short term, the model may characterize early failures and burn-in testing times. In the long run, the hazard function behaves similar to the hazard function of the exponential distribution.

Corollary 4. The mean time to failure (MTTF) given by

$$MTTF = \int_0^\infty sf(s)ds = \int_0^\infty R(s)ds \tag{21}$$

is not analytically available.

Proof. Note that

$$\begin{aligned}\text{MTTF} &= \int_0^\infty sf(s)ds\\ &= \int_0^\infty s\lambda\left(\mathrm{e}^{\phi t} + \phi t - 1\right)\mathrm{e}^{-\lambda t-\phi t+\lambda t\mathrm{e}^{-\phi t}}ds\end{aligned} \tag{22}$$

And

$$\begin{aligned}\text{MTTF} &= \int_0^\infty R(s)ds\\ &= \int_0^\infty \mathrm{e}^{-\lambda t+\lambda t\mathrm{e}^{-\phi t}}ds\end{aligned} \tag{23}$$

Have no antiderivative. Another consequence of Corollary 4 is that the moment-generating function is not available analytically.

Corollary 5. The maximum likelihood estimators of the NTA reliability parameters are given by

$$\lambda = -\frac{n}{\sum_{i=1}^n t_i\mathrm{e}^{-\phi t_i} - t_i}. \tag{24}$$

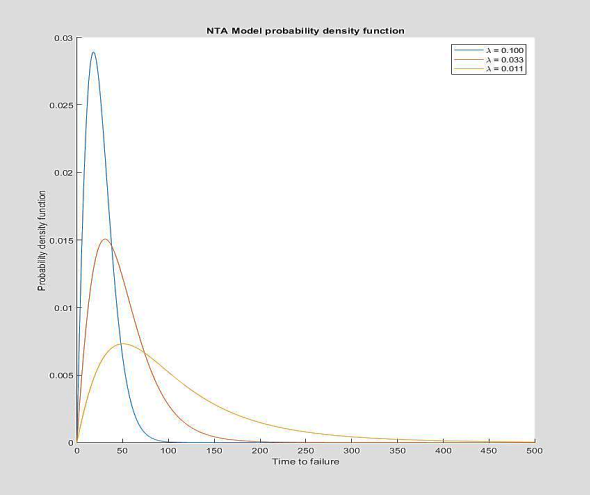

Figure 3: Neyman type A probability density functions.
Source: Authors.

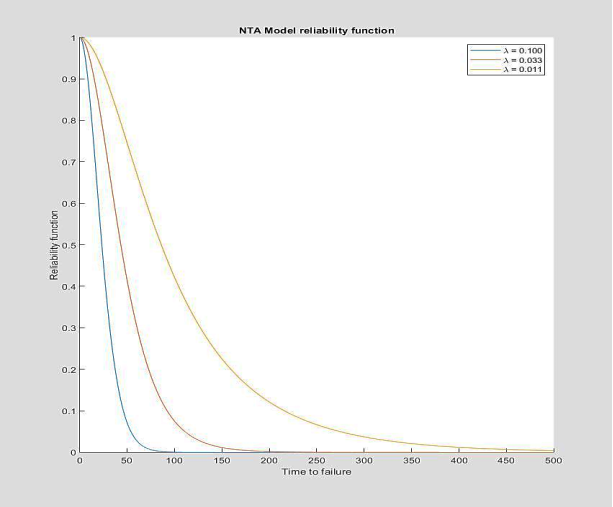

Figure 4 Neyman type A reliability functions.
Source: Authors.

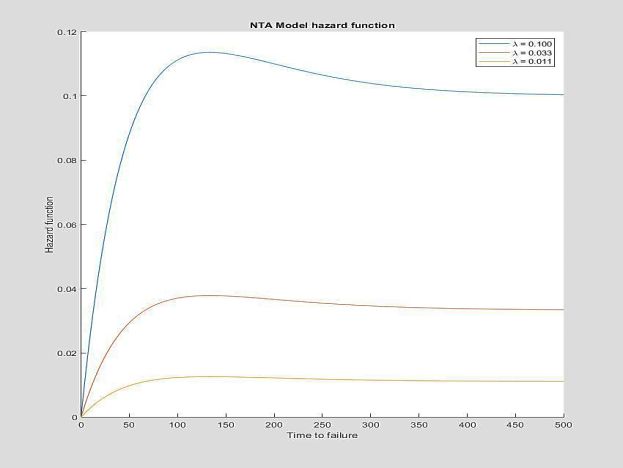

Figure 5: Neyman type A hazard rate functions.
Source: Authors.

And

$$\sum_{i=1}^{n} \frac{t_i e^{\phi t_i} + t_i}{e^{\phi t_i} + \phi t_i - 1} - \sum_{i=1}^{n} \lambda t_i^2 + e^{-\phi t_i} + t_i = 0. \tag{25}$$

An estimator for ϕ is not analytically available. Its approximation is given by the numerical solution of nonlinear equation (25).

Proof. Given a random sample $t_1, t_2, \ldots, t_n$, the maximum likelihood estimators of the NTA lifetime density function with parameters (λ, ϕ) are obtained by finding $\frac{\partial \mathcal{L}}{\partial \lambda} = 0$ and $\frac{\partial \mathcal{L}}{\partial \phi} = 0$ [32]. Then, the likelihood function for n non-censored data points is given by

$$L = \prod_{i=1}^{n} \lambda\left(e^{\phi t_i} + \phi t_i - 1\right) e^{-\lambda t_i - \phi t_i + \lambda t_i e^{-\phi t_i}}. \tag{26}$$

We have that

$$L = \lambda^n \prod_{i=1}^{n} \left(e^{\phi t_i} + \phi t_i - 1\right) e^{-\lambda t_i - \phi t_i + \lambda t_i e^{-\phi t_i}} \tag{27}$$

Putting $\mathcal{L} = \ln(L)$, then,

$$\begin{aligned} \mathcal{L} = n \ln \lambda + \sum_{i=1}^{n} \ln\left(e^{\phi t_i} + \phi t_i - 1\right) \\ + \sum_{i=1}^{n} \lambda t_i e^{-\phi t_i} - \lambda t_i - \phi t_i \end{aligned} \tag{28}$$

Finding the extreme points of 27] we have

$$\frac{\partial \mathcal{L}}{\partial \lambda} = \frac{n}{\lambda} - \sum_{i=1}^{n} t_i e^{-\phi t_i} - t_i = 0. \tag{29}$$

So, the maximum likelihood estimator for the parameter λ is given by

$$\lambda = -\frac{n}{\sum_{i=1}^{n} t_i e^{-\phi t_i} - t_i}. \tag{30}$$

Following from (27) we have

$$\frac{\partial \mathcal{L}}{\partial \phi} = \sum_{i=1}^{n} \frac{t_i e^{\phi t_i} + t_i}{e^{\phi t_i} + \phi t_i - 1} - \sum_{i=1}^{n} \lambda t_i^2 + e^{-\phi t_i} + t_i = 0. \tag{31}$$

Note that estimator (31) for ϕ is not available analytically. By substituting (30) into (31), the approximation for ϕ is given by the numerical solution of the following nonlinear equation:

$$\begin{aligned} \sum_{i=1}^{n} \frac{t_i e^{\phi t_i} + t_i}{e^{\phi t_i} + \phi t_i - 1} + \\ \sum_{i=1}^{n} \left(\frac{n}{\sum_{i=1}^{n} t_i e^{-\phi t_i} - t_i}\right) t_i^2 - e^{-\phi t_i} - t_i = 0. \end{aligned} \tag{32}$$

Suppose the failure times of a product follow the NTA distribution with parameters $\phi = 0.015$. In addition, we consider that the manufacturer's cost c_0 for the given product equals unity. The warranty cost for renewing the free replacement warranty for a period of W is given by

$$\mathbb{E}[C(W)] = \frac{c_0 F(W)}{1 - F(W)} = \frac{c_0\left(1 - \mathrm{e}^{-\lambda W + \lambda W \mathrm{e}^{-\phi W}}\right)}{\mathrm{e}^{-\lambda W + \lambda W \mathrm{e}^{-\phi W}}}. \quad (33)$$

Fig. 6 depicts the warranty cost for a renewing free replacement warranty [4] for various warranty periods by varying parameter λ. As predicted, the value of λ that produces the lowest reliability or largest hazard function, as illustrated in Fig.6, produces the highest warranty costs.

4 Arrhenius-NTA model for accelerated tests

Let a quantifiable life measure G implied by the Arrhenius law be given by

$$G(V) = C\mathrm{e}^{\frac{B}{V}}. \quad (34)$$

The Arrhenius relationship is a physics-based model derived for the temperature life dependence, V, in Kelvin. It is a widely used model to relate the product life and temperature [3]. In Equation (34), C is a nonthermal constant that depends on geometry, size, fabrication, and other factors. It is determined experimentally, and deals with the frequency of molecules that collide in the correct orientation to initiate a chemical reaction. Parameter B is the relationship between the activation energy and Boltzmann Constant. The activation energy deals with the magnitude of the effect of the stress on the component. The details can be found in [3] and [1].

Let the probability density function of life data be given by (11). Let the inverse scale parameter λ be equal to the quantifiable life measure of Arrhenius law. Setting $G(V) = \lambda$ we have the Arrhenius-NTA probability density function:

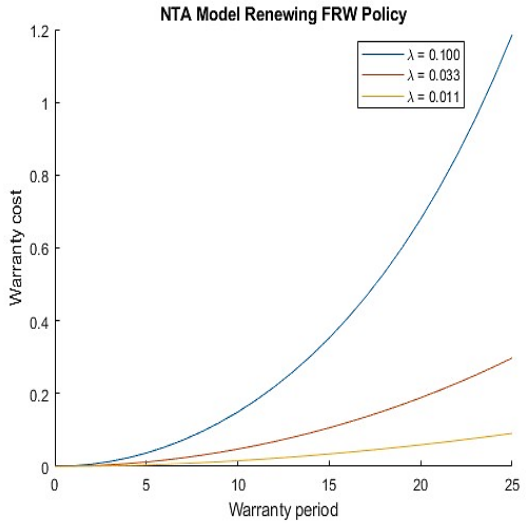

Figure 6. Hazard function.
Source: Authors.

$$f(t,V) = C\mathrm{e}^{\frac{B}{V}}\left(\mathrm{e}^{\phi t} + \phi t - 1\right)\mathrm{e}^{-C\mathrm{e}^{\frac{B}{V}}t - \phi t + C\mathrm{e}^{B}t\mathrm{e}^{-\phi t}}. \quad (35)$$

The probability density function (35) has the following important characteristics: It is shown that the model is qualitatively suitable for investigating the fluorescent bulb lifespan in cold weather, the toughness of steels, and the Ductile to Brittle Transition Temperature. We have that

$$R(t,V) = \mathrm{e}^{-C\mathrm{e}^{\frac{B}{V}}t + C\mathrm{e}^{\frac{B}{V}}t\mathrm{e}^{-\phi t}}, \quad (36)$$

and

$$h(t,V) = C(\mathrm{e}^{\varphi t} + \varphi t - 1)\mathrm{e}^{\frac{B}{V} - \varphi t}. \quad (37)$$

The probability density functions 35, 46, and 37 are depicted in Figs. 7, 8 and 9 for the parameters $C = 0.0002, B = 1000$ and $\phi = 0.0025$. Note that in the brittle fatigue of metals for a fixed mechanical load, the lower the temperature, the higher is the chance of failure. The resulting positive slope of the short end of the hazard function describes the gradual decrease in load resistance well.

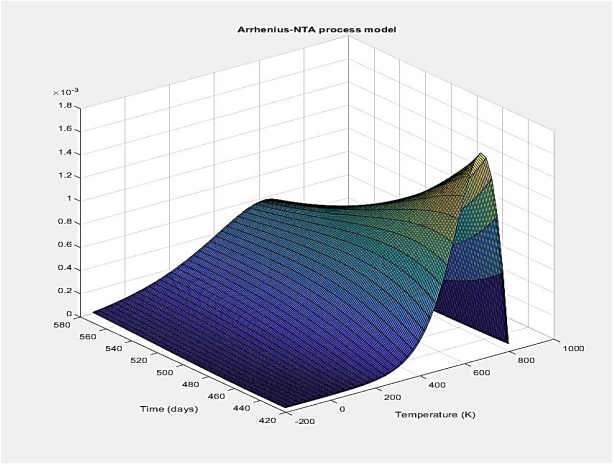

Figure 7. Probability density function.
Source: Authors.

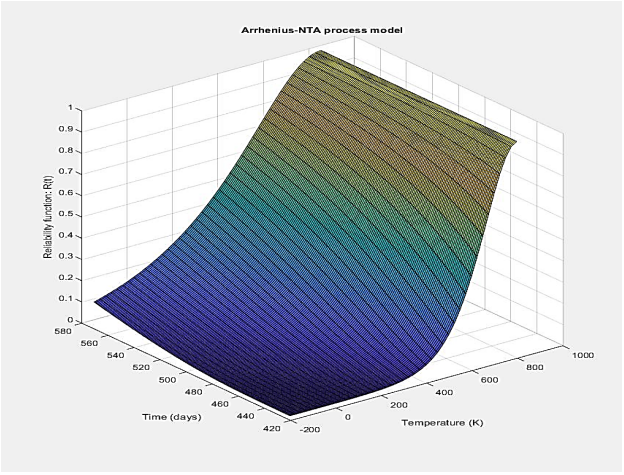

Figure 8. Reliability function.
Source: Authors.

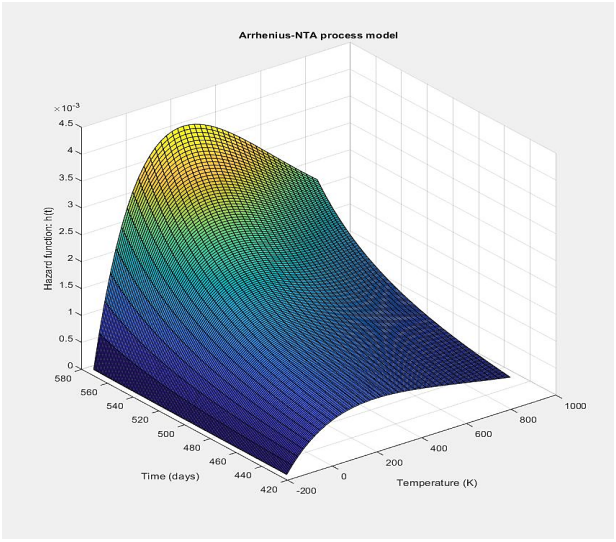

Figure 9. Hazard function.
Source: Authors.

The hazard function inherits the NTA model hump-shaped properties.

Corollary 6. The Arrhenius-NTA hazard function (37) is a humped model.

Proof. Note that the derivative of the hazard function given by:

$$\frac{\partial h(t,V)}{\partial t} = -C\phi(\phi t - 2)\mathrm{e}^{\frac{B}{V}-\phi t} \tag{38}$$

finds root at $t^* = \frac{2}{\phi}$. Since that $\lambda > 0$, and

$$\frac{\partial^2 h(t,V)}{\partial t^2} = C\phi^2(\phi t - 3)\mathrm{e}^{\frac{B}{V}-\phi t}, \tag{39}$$

we have that

$$\frac{\partial^2 h(t^*,V)}{\partial t^2} = -C\phi^2\lambda\mathrm{e}^{\frac{B}{V}-2}. \tag{40}$$

So, the Arrhenius-NTA hazard function finds its maximum at t^*.

Corollary 7. The Arrhenius-NTA hazard function (37) increases as the stress V decreases.

Proof. If the hazard function is given by

$$h(t,V) = C(\mathrm{e}^{\varphi t} + \varphi t - 1)\mathrm{e}^{\frac{B}{V}-\varphi t}, \tag{41}$$

then

$$\begin{aligned} &\lim_{V\to 0} C(\mathrm{e}^{\varphi t} + \varphi t - 1)\mathrm{e}^{\frac{B}{V}}\mathrm{e}^{-\varphi t} \\ &C(\mathrm{e}^{\varphi t} + \varphi t - 1)\mathrm{e}^{-\varphi t}\lim_{V\to 0}\mathrm{e}^{\frac{B}{V}} \\ &C(\mathrm{e}^{\varphi t} + \varphi t - 1)\mathrm{e}^{-\varphi t}\lim_{V\to 0}\mathrm{e}^{\frac{B}{V}} = \infty \end{aligned} \tag{42}$$

Corollary 7 shows that the hazard function of the Arrhenius-NTA model is inversely proportional to stress. This is precisely the behavior of metallic materials. In general, the increase in the tensile and yield strengths at low temperatures is characteristic of metals. However, it is important to note that it is not claimed here that every metallic material can be fitted better by the Arrhenius-NTA reliability distribution. The modeling gain must be tested in each case.

Corollary 8. The Arrhenius-NTA hazard function converges to $C\mathrm{e}^{\frac{B}{V}}$ in the long run. Proof. If the hazard function is given by:

$$h(t,V) = C(\mathrm{e}^{\varphi t} + \varphi t - 1)\mathrm{e}^{\frac{B}{V}-\varphi t}, \tag{43}$$

then

$$\begin{aligned} &\lim_{t\to\infty} C\mathrm{e}^{\frac{B}{V}}(\mathrm{e}^{\varphi t} + \varphi t - 1)\mathrm{e}^{-\varphi t} \\ &C\mathrm{e}^{\frac{B}{V}}\lim_{t\to\infty}(\mathrm{e}^{\varphi t} + \varphi t - 1)\mathrm{e}^{-\varphi t} \\ &C\mathrm{e}^{\frac{B}{V}}\lim_{t\to\infty}\left(1 + \phi t\mathrm{e}^{-\phi t} - \mathrm{e}^{-\phi t}\right) \\ &C\mathrm{e}^{\frac{B}{V}}\left(\lim_{t\to\infty} 1 + \lim_{t\to\infty}\phi t\mathrm{e}^{-\phi t} - \lim_{t\to\infty}\mathrm{e}^{-\phi t}\right) \\ &C\mathrm{e}^{\frac{B}{V}}\left(1\lim_{t\to\infty} 1 + 0\lim_{t\to\infty}\phi t\mathrm{e}^{-\phi t} - 0\lim_{t\to\infty}\mathrm{e}^{-\phi t}\right) = C\mathrm{e}^{\frac{B}{V}} \end{aligned} \tag{44}$$

As in Corollary 4, the MTTF of the Arrhenius-NTA is not analytically available. Figs. 10 and 11 show the numerically solved mean time to failure (MTTF) of the Arrhnenius-NTA model.

The solution can be obtained by

$$MTTF = \int_0^\infty sC\mathrm{e}^{\frac{B}{V}}\big(\mathrm{e}^{\phi s} + \phi s - 1\big)\mathrm{e}^{-C\mathrm{e}^{\frac{B}{V}}s-\phi s+C\mathrm{e}^{\frac{B}{V}}s\mathrm{e}^{-\phi s}}ds \tag{45}$$

Or

$$MTTF = \int_0^\infty \mathrm{e}^{-C\mathrm{e}^{\frac{B}{V}}s+C\mathrm{e}^{\frac{B}{V}}s\mathrm{e}^{-\phi s}}ds, \tag{46}$$

which is the expected value of the random variable t or integration through the entire domain of the survival function. The MTTF can also be achieved through simulation, as introduced in the next section. It was shown that lower temperatures and higher activation energies decreased the MTTF of the component under test. A large activation energy indicates that stress has a substantial effect on MTTF.

Lower values of C and ϕ had a greater influence on the effect of temperature on the life of the component. When fixed, the parameters were $C = 0.002$ and $\phi = 0.0025$.

Corollary 9. The maximum likelihood estimators of the Arrhenius-NTA reliability parameters are given by:

$$C = -\frac{\sum_{i=1}^n \mathrm{e}^{\phi t_i}}{\sum_{i=1}^n t\mathrm{e}^{\phi t_i+\frac{B}{V}} - \mathrm{e}^{\frac{B}{V}}t_i}, \tag{47}$$

$$\frac{\partial \mathcal{L}}{\partial B} = \sum_{i=1}^n \frac{Ct_i\mathrm{e}^{\frac{B}{V}-\phi t_i}}{V} - \frac{Ct_i\mathrm{e}^{\frac{B}{V}}}{V} + \frac{n}{V} \tag{48}$$

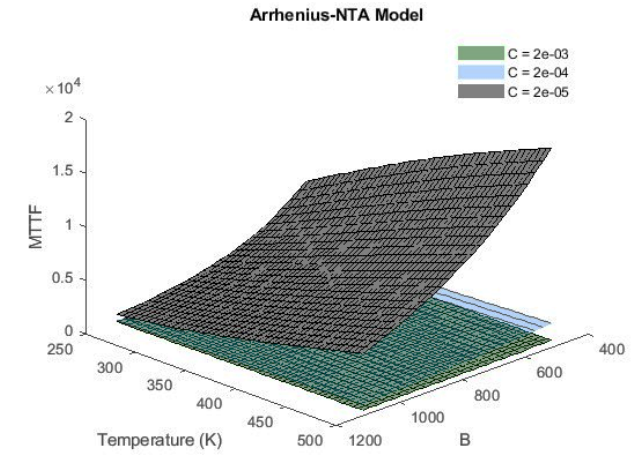

Figure 10. Mean time to failure varying parameter C.
Source: Authors.

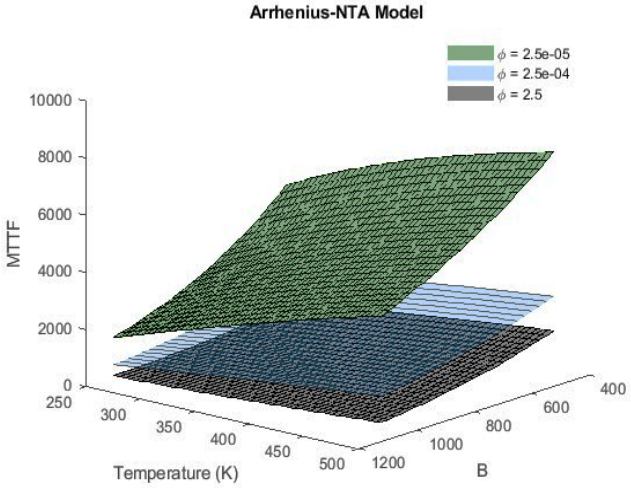

Figure 11. Mean time to failure varying parameter ϕ.
Source: Authors.

and

$$\frac{\partial \mathcal{L}}{\partial \phi} = \sum_{i=1}^{n} - Ct_i^2 \mathrm{e}^{\frac{B}{V} - t_i\varphi} + \frac{t_i \mathrm{e}^{t_i\varphi} + t_i}{\mathrm{e}^{t_i\varphi} + t_i\varphi - 1} - t_i = 0. \quad (49)$$

Estimators for B and ϕ are not analytically available. Their approximations are given by the numerical solution of the nonlinear Equations 48) and (49), respectively.

Proof. Given a random sample $t_1, t_2, \ldots, t_n$, the maximum likelihood estimators of the Arrhenius-NTA lifetime density function with parameters (C, B, ϕ) are obtained by finding $\frac{\partial \mathcal{L}}{\partial C} = 0, \frac{\partial \mathcal{L}}{\partial B} = 0$ and $\frac{\partial \mathcal{L}}{\partial \phi} = 0$ [32]. Then, the likelihood function for n non-censored data points is given by

$$L = \prod_{i=1}^{n} C\mathrm{e}^{\frac{B}{V}} \left(\mathrm{e}^{\phi t_i} + \phi t_i - 1\right) \mathrm{e}^{-C\mathrm{e}^{\frac{B}{V}} t_i - \phi t_i + C\mathrm{e}^{\frac{B}{V}} t_i \mathrm{e}^{-\phi t_i}}. \quad (50)$$

We have that

$$L = \left(C\mathrm{e}^{\frac{B}{V}}\right)^n \prod_{i=1}^{n} \left(\mathrm{e}^{\phi t_i} + \phi t_i - 1\right) \mathrm{e}^{-C\mathrm{e}^{\frac{B}{V}} t_i - \phi t_i + C\mathrm{e}^{\frac{B}{V}} t_i \mathrm{e}^{-\phi t_i}}$$

$$\mathcal{L} = \ln(L) = n \ln\left(C\mathrm{e}^{\frac{B}{V}}\right) + \sum_{i=1}^{n} \ln\left(\mathrm{e}^{\phi t_i} + \phi t_i - 1\right) + \sum_{i=1}^{n} \left(C\mathrm{e}^{\frac{B}{V}}\right) t_i \mathrm{e}^{-\phi t_i} - \left(C\mathrm{e}^{\frac{B}{V}}\right) t_i - \phi t_i \quad (51)$$

Finding the extreme points of (51) in terms of C we have

$$\frac{\partial \mathcal{L}}{\partial C} = \frac{n}{C} + \sum_{i=1}^{n} t_i \mathrm{e}^{\frac{B}{V} - \phi t} - \mathrm{e}^{\frac{B}{V}} t_i = 0. \quad (52)$$

So, the maximum likelihood estimator for the parameter C is given by

$$C = -\frac{n}{\sum_{i=1}^{n} t_i \mathrm{e}^{\frac{B}{V} - \phi t_i} - \mathrm{e}^{\frac{B}{V}} t_i}. \quad (53)$$

Finding the extreme points of (51) in terms of B we have

$$\frac{\partial \mathcal{L}}{\partial B} = \frac{n}{V} + \sum_{i=1}^{n} \frac{Ct_i \mathrm{e}^{\frac{B}{V} - \phi t_i}}{V} - \frac{Ct_i \mathrm{e}^{\frac{B}{V}}}{V} = 0. \quad (54)$$

Finding the extreme points of (51) in terms of ϕ we have

$$\frac{\partial \mathcal{L}}{\partial \phi} = \sum_{i=1}^{n} - Ct_i^2 \mathrm{e}^{\frac{B}{V} - t_i\varphi} + \frac{t_i \mathrm{e}^{t_i\varphi} + t_i}{\mathrm{e}^{t_i\varphi} + t_i\varphi - 1} - t_i = 0. \quad (55)$$

Note that estimators (54) for B and (55) for ϕ are not analytically available.

4.1 Simulation

In the following tables, we present the estimated parameters and value of the log-likelihood function. Notably, the relative error decreased as the sample size increased. The true parameters are by *V=300, C=0.0002, B=1000* and $\phi = 0.0025$. The expected number of failures in an interval of time is calculated using the renewal process, which is associated with the distribution function $F(t) = 1 - R(t).M(t)$ given by

$$M(t) = F(t) + \int_0^t \left[\sum_{r=1}^{\infty} F_r(t-x)\right] f(x)dx, \quad (56)$$

is called the renewal function, and was discussed by [1]. The function $M(t)$ is difficult to obtain in analytical form, but an efficient numerical approximation can be found in [33].

Table 1.
MLE estimators for $n = 30$.

Parameter	Estimation	Relative Error
C	0.000028665638	0.856
B	1437	0.437
ϕ	0.006615886708	1.646
$\mathcal{L}$	200.57	0.0046

Source: Authors.

Table 2.
MLE estimators for *n=300*

Parameter	Estimated	Relative Error
C	0.000250776105	0.253
B	1335	0.335
ϕ	0.000420982926	0.831
$\mathcal{L}$	1939	0.0032

Source: Authors.

Table 3.
MLE estimators for $n = 900$.

Parameter	Estimated	Relative Error
C	0.000204747157	0.023
B	1163	0.163
ϕ	0.001189293500	0.524
$\mathcal{L}$	5792	0.0015

Source: Authors.

As shown in Tables 4 and 5, the expected number of failures in $t \in (0,1000)$ for a set of selected temperatures and parameter B of the Arrhenius-NTA model (35). The base parameters are $V = 300, B = 1000$ and $\phi = 0.0025$. It is clear that, confirming the above results, the expected number of failures increased as V decreased. The opposite was true for parameter B.

The approximation of the renewal function is particularly useful for calculating the warranty costs and maintenance policies.

Table 4.
Expected number of failures for $t = 1000$.

Temperature (K)	$M(t)$
250	4.73
300	3.07
350	2.19
400	1.67

Source: Authors.

4.2 Application procedure

This procedure outlines the application of the Neyman Type A reliability model to analyze the failure of metallic materials under low-temperature conditions. The model is particularly useful for understanding and predicting the failure behavior of metals subjected to extreme thermal stresses.

Table 5.
Expected number of failures for $t = 1000$.

Parameter B	$M(t)$
700	1.469
800	1.904
900	2.434
1000	3.071

Source: Authors.

- Identify the parameters: The fundamental parameters for this model include the operating temperature and fixed applied mechanical stress.
- The experimental failure data of the material were collected at various temperatures to capture the variation in the failure rate with temperature.
- Apply the Neyman Type A distribution to the collected data to estimate the model parameters and the material survival function using the maximum likelihood estimators given by Equations (47), (48), and (49).
- The estimated survival function (36) was used to predict the reliability of the material under defined operational conditions.
- Equations (45) or (46) were used to estimate the mean time to failure.

To validate the model, a comparison of the reliability predictions with the actual failure data obtained under controlled operational conditions must be conducted as well as a sensitivity analysis to understand the impact of each parameter on the model and refine the application procedure based on these insights.

5 Discussion

The application of the Neyman Type A distribution is especially pertinent in engineering contexts where material failures at low temperatures are critical. This scenario is often encountered in metallic structures and components used in extremely cold environments such as polar regions, aerospace applications, and equipment employed in low-temperature chemical processes. These conditions are noteworthy for inducing brittleness and fatigue in metals, phenomena that occur when materials are exposed to temperatures below their ductile–brittle transition point. In such scenarios, conventional failure characteristics observed at normal or elevated temperatures do not apply, rendering traditional reliability analyses insufficient.

With its ability to model failure behaviors in multimodal distributions, the Neyman Type A distribution is a valuable

statistical tool for predicting the reliability of these materials under reduced thermal stress conditions. For instance, aircrafts operating at high altitudes encounter extremely low temperatures that can compromise the integrity of metallic components, necessitating a reliability model that can adequately predict the likelihood of failure. Similarly, in polar regions, engineering structures and equipment must withstand not only intense cold, but also significant temperature variations, which can adversely affect their performance and durability.

The implementation of a model based on the Neyman Type A distribution in engineering projects allows designers and engineers to conduct more refined and accurate assessments of the reliability and performance of materials and components under low-temperature conditions. By integrating this model into the design processes, it is possible to simulate the failure behavior of materials over time and under various environmental stress conditions, leading to improvements in material selection, structural design, and maintenance strategies. By quantifying the failure risk more accurately, engineers can optimize the design to withstand adverse conditions and enhance the safety and efficiency. Furthermore, the model can be employed to develop accelerated testing plans, helping to identify weaknesses in engineering designs and ensuring that selected materials meet the durability and reliability requirements before large-scale implementation. This not only extends the lifespan of components, but also reduces maintenance and replacement costs, significantly contributing to the sustainability and economic efficiency of engineering projects.

Therefore, the selection of the Neyman Type A distribution for this study is grounded in the necessity of a statistical model that can accurately reflect the peculiarities of failures at low temperatures, allowing for a more precise and reliable analysis of the lifespan and failure behavior of metallic materials in these demanding contexts.

6 Conclusion

In this study, we introduced a novel statistical model utilizing the Neyman Type A distribution for reliability analysis, specifically tailored to address the challenges of modeling material failures at low temperatures. The development of the model was driven by the need to understand and predict the brittle fracture of metals under cold conditions, a scenario that is often overlooked in conventional reliability engineering. Through our research, we have not only demonstrated the humped behavior of the hazard function and its convergence to a constant rate λ, but also highlighted the utility of the model in accurately describing the inversely proportional relationship between failure risk and stress. This unique characteristic underscores the significance of the model in engineering applications in which low-temperature performance is critical.

Our findings align closely with the initial objectives of this study, providing a robust framework for analyzing the reliability of materials in environments subjected to thermal stress. The predictive capacity of the model for early failure and its behavior under varying stress conditions offers substantial advancement in the field of reliability engineering. Future research directions include testing the model against alternative stress scenarios, conducting sensitivity analyses of the parameters, and validating the model with experimental data to enhance its comparability with the existing models. Additionally, exploring the interaction between mechanical load and temperature in a nonthermal life-stress relationship model presents an exciting avenue for extending the applicability of our work. This study not only fills a gap in the existing literature, but also sets the stage for more comprehensive and accurate reliability assessments in engineering disciplines concerned with low-temperature material performance.

References

[1] Elsayed, E.A., Reliability Engineering, Wiley Series in Systems Engineering and Management, 3rd Ed., Wiley. 2021. DOI: https://doi.org/10.1002/9781119665946.

[2] Deshpande, J.V. and Purohit, S.G., Lifetime data: statistical models and methods, Series on quality, reliability and engineering statistics, World Scientific. 2005. DOI: https://doi.org/10.1142/5988.

[3] Nelson, W., Accelerated testing: statistical models, test plans, and data analyses, 2nd Ed., John Wiley & Sons, 2004.

[4] Wallace, R., Blischke, M., Rezau-Karim, D.N.P.M., Warranty data collection and analysis, Springer Series in Reliability Engineering, Springer, 2011. DOI: https://doi.org/10.1007/978-0-85729-647-4.

[5] Rahman, A., and Chattopadhyay, G., Long term warranty and after sales: service concept, policies and cost models, Springer Briefs in Applied Sciences and Technology, Springer, 2015. DOI: https://doi.org/10.1007/978-3-319-16271-3.

[6] Murthy, D.N.P., and Jack, N., Extended warranties, maintenance Service and lease contracts: modeling and analysis for decision-making, Springer Series in Reliability Engineering, Springer, 2014. DOI: https://doi.org/10.1007/978-1-4471-6440-1.

[7] Smith, R., and Mobley, R.K., Rules of thumb for maintenance and reliability engineers, Elsevier, 2008.

[8] da Silva, A.J., Maintenance policy costs considering imperfect repairs. Reliability: Theory & Applications. 1(72), pp. 564-574, 2023. DOI: https://doi.org/10.24412/1932-2321-2023-172-564-574

[9] de Souza, F.L.C., da Silva, A.J., Statistical learning for maintenance optimization: modeling the hazard function with variable recovery factors. Revista de Gestão e Secretariado, 15(2), art. e3478, 2024. DOI: https://doi.org/10.7769/gesec.v15i2.3478

[10] Lee, J.M., Special issue: Low-temperature behavior of metals, Metals 12(4), 2022.

[11] Xi, X., Zhao, D.Q., Pan, M.X., Wang, W., Wu, Y., and Lewandowski, J.J., Fracture of brittle metallic glasses: Brittleness or plasticity. 2005. DOI: https://doi.org/10.1103/PhysRevLett.94.125510

[12] Lancaster, J., Chapter 4 - The technical background, in: Lancaster, J., ed., Engineering Catastrophes, 3rd Ed., Woodhead Publishing, 2005, pp. 139-189. DOI: https://doi.org/10.1533/9781845690816.

[13] Chernov, V., Kardashev, B., and Moroz, K., Low-temperature embrittlement and fracture of metals with different crystal lattices dislocation mechanisms, Nuclear Materials and Energy 9, 496-501. 2016. DOI: https://doi.org/10.1016/j.nme.2016.02.002.

[14] Sallaba, F., Rolof, F., Ehlers, S., Walters, C.L., and Braun, M., Relation between the fatigue and fracture ductile-brittle transition in s500 welded steel joints, Metals 12(3), art. 305, 2022. DOI: https://doi.org/10.3390/met12030385

[15] Park, J.Y., Kim, B.K., Nam, D.G., and Kim, M.H., Effect of nickel contents on fatigue crack growth rate and fracture toughness for nickel alloy steels, Metals 12(2), art. 173, 2022. DOI: https://doi.org/10.3390/met12020173

[16] Mulford, R.A., Grain-boundary embrittlement of ni and ni alloys, in C. Briant and Banerji, S., Ed., Embrittlement of Engineering Alloys, Vol. 25 of Treatise on Materials Science & Technology, Elsevier, pp. 1-19. 1983. DOI: https://doi.org/10.1557/S0883769400069001.

[17] Lepov, V., Grigoriev, A., Achikasova, V., and Lepova, K., Cold resistance of materials as an integrity factor of railway transport in the

extreme environment, in Procedia Structural Integrity: 1st International Conference on Integrity and Lifetime in Extreme Environment, Vol. 20, 2019, pp. 57-62. DOI: https://doi.org/10.1016/j.prostr.2019.12.116.
[18] Li, Y., Fu, G., Wan, B., Jiang, M., Zhang, W., and Yan, X., Failure analysis of sac305 ball grid array solder joint at extremely cryogenic temperature, Applied Sciencies 10, 2020. DOI: https://doi.org/10.3390/app10061951.
[19] Bo-Bonning, C., Blackburn, J., Stretz, H.A., Wilson, C.D., Johnson, W.R., Superposition-based predictions of creep for polymer films at cryogenic temperatures, Cryogenics, 104, art. 102979, 2019. DOI: https://doi.org/10.1016/j.cryogenics.2019.102979.
[20] Soares, G.C., Rodrigues, M.C.M., and Santos, L.deA., Influence of temperature on mechanical properties, fracture morphology and strain hardening behavior of a 304 stainless steel. Materials Research, 20, pp. 141–151, 2017. DOI: https://doi.org/10.1590/1980-5373-MR-2016-0932
[21] Mohsin-Sattar, A.R., Othman, S., Kamaruddin, M.A., and Rashid, K., Limitations on the computational analysis of creep failure models: a review. Engineering Failure Analysis, 134, art. 105968 2022. DOI: https://doi.org/10.1016/j.engfailanal.2021.105968.
[22] Hossain, M.A., and Stewart, C.M., A probabilistic creep model incorporating test condition, initial damage, and material property uncertainty. International Journal of Pressure Vessels and Piping. 193, art. 104446, 2021. DOI: https://doi.org/10.1016/j.ijpvp.2021.104446.
[23] Chandra, K., Kain, V., Bhutani, V., Raja, V.S., Tewari, R., Dey, G.K., and Chakravartty, J.K., Low temperature thermal aging of austenitic stainless-steel welds: kinetics and effects on mechanical properties. DOI: https://doi.org/10.1016/j.msea.2011.11.055
[24] Run-Zi, W., Hang-Hang G., Shun-Peng Z., Kai-Shang L., Ji W., Xiao-Wei W., Miura, H., Xian-Cheng Z., and Shan-Tung T., A data-driven roadmap for creep-fatigue reliability assessment and its implementation in low-pressure turbine disk at elevated temperatures. Reliability Engineering & System Safety, 225, art. 108523, 2022. DOI: https://doi.org/10.1016/j.ress.2022.108523.
[25] Neyman, J., On a new class of contagious distributions applicable in entomology and bacteriology, Ann. Math. Stat 10, pp. 35-57, 1939. DOI: https://doi.org/10.1214/aoms/1177732245.
[26] Martin, D.C., and Katti, S.K., Approximations to the neyman type a distribution for practical problems, Biometrics 18(3), pp. 354-364, 1962. DOI: https://doi.org/10.2307/2527477.
[27] Ozel, G., and Turkan, S., Neyman type a distribution for the natural disasters and related casualties in Turkey, Journal of Data Science 13(3), pp. 533-550, 2022. DOI: https://doi.org/10.6339/JDS.201507_13(3).0007.
[28] Johnson, N.L., Kemp, A.W., and Kotz, S., Univariate discrete distributions, Wiley Series in Probability and Statistics, 3rd Ed., Wiley. 2005. DOI: https://doi.org/10.1002/0471715816.
[29] Fang, F., and Oosterlee, C.W., A novel pricing method for European options based on Fourier-cosine series expansions, SIAM Journal on Scientific Computing 31(2), pp. 826-848, 2009. DOI: https://doi.org/10.1137/080718061.
[30] da Silva, A.J., Baczynski, J., and Vicente, J.V.M., Recovering probability functions with Fourier series. Pesquisa Operacional, 43, art. 7882 2023. DOI: https://doi.org/10.1590/0101-7438.2023.043.00267882
[31] Shenton, L.R. and Bowman, K.O., Remarks on large sample estimators for some discrete distributions, technometrics, Technometrics 9(4), pp. 587-598,1967. DOI: https://doi.org/10.2307/1266197.
[32] Fisher, R.A., On the mathematical foundations of theoretical statistics, Philosophical Transactions of the Royal Society of London 222, pp. 309-368, 1922. DOI: https://doi.org/10.1098/rsta.1922.0009.
[33] Sasongko, L. and Mahatma, T., The estimation of renewal functions using the mean value theorem for integrals (mevti) method. d'CARTESIAN 5, pp. 111-120, 2016. DOI: https://doi.org/10.35799/dc.5.2.2016.14984.

A.J. Da Silva, received the BSc. Eng. in Production Engineering from the Catholical University of Petropolis (UCP), Petropolis, Rio de Janeiro - Brazil, in 2012. MSc. and PhD. in Computational Modeling from the National Laboratory for Scientifical Computing (LNCC), Petropolis, Rio de Janeiro - Brazil, in 2015 and 2021, respectively. Since 2016, he has been a Professor with the Production Engineering Department, CEFET/RJ, Itaguai, Rio de Janeiro - Brazil. His research interests include numerical methods, stochastic processes, reinforcement learning, reliability engineering, and quantitative finance applications.
ORCID: 0000-0001-9763-6395

F.DoC. Amorim, holds a BSc in 2013, MSc. In 2015, and PhD. In 2018, in Mechanical Engineering from the Fluminense Federal University (UFF), Brazil. He is a Sp. in Radiological Protection and Safety of Radioactive Sources in 2018, from the Institute of Radioprotection and Dosimetry (IRD/CNEN) in partnership with the International Atomic Energy Agency (IAEA). Currently, he is a professor at the Federal Center for Technological Education Celso Suckow da Fonseca (Cefet/RJ), working in the Department of Mechanical Engineering and in the Graduate Program in Mechanical Engineering and Materials Technology (PPEMM). He has experience in the field of mechanical engineering, with an emphasis on solid, elastic, and plastic body mechanics, focusing mainly on the following topics: industrial maintenance, structural integrity, mechanical behavior of materials, mechanics of composite materials, and polymers. Hewas awarded the Young Scientist of Our State (JCNE) - FAPERJ - 2022. He currently serves as the Coordinator of the Coordination of Research and Technological Studies (COPET) at Cefet/RJ.
ORCID: 0000-0001-6658-0106